Effects of Volumetric Modes on the Optimization of Micro-Perforated Multi-Layer Absorber Panels

Cédric Maury, Teresa Bravo, Daniel Mazzoni, Muriel Amielh

Effects of Volumetric Modes on the Optimization of Micro-Perforated Multi-Layer Absorber Panels

C. Maury [a], T. Bravo [b], D. Mazzoni [c] and M. Amielh [c]

[a] Laboratory of Mechanics and Acoustics (LMA CNRS), Ecole Centrale Méditerranée, 4 impasse Nikola Tesla, F-13013 Marseille, France
[b] Institute for Physical and Information Technologies (ITEFI), Spanish National Research Council (CSIC), Serrano 144, 28006 Madrid, Spain
[c] Institute of Research on Non-Equilibrium Phenomena (IRPHE CNRS), 49 rue Frédéric Joliot-Curie, F-13013 Marseille, France

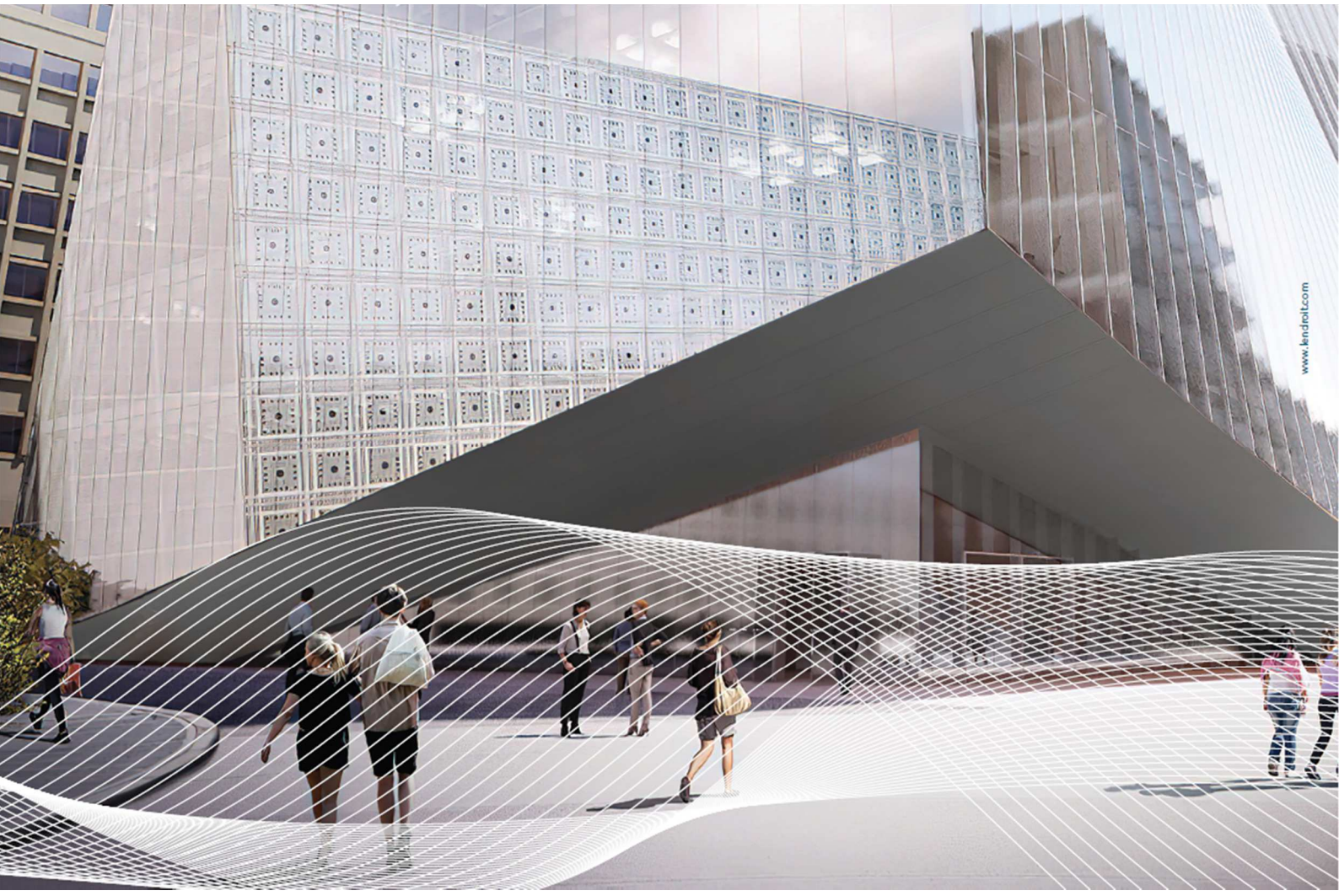

Acoustic wall-treatments composed of thin, lightweight micro-perforated multilayer panels (MPMPs) offer a potential solution for broadband absorption of ambient noise, with applications in building acoustics and transport systems requiring constraints on mass and thickness. A MPMP with a negative porosity gradient, induced by a decrease in perforation diameters, can ensure, after optimization, absorption greater than 0.9 over three octaves beyond 140 Hz, while maintaining sub-wavelength thickness. However, such a configuration presents practical limitations linked to the vibrating response of thin panels, which can degrade the broadband performance, and also to the difficulty of producing cylindrical micro-perforations with diameters less than 200 microns on millimetric thicknesses. This study examines the effect of the first volumetric modes of thin micro-perforated plates on the absorption, reflection and transmission loss of functionally-graded MPMPs. The optimization effort focuses on the distance between perforations, rather than their diameter, as well as on the depth of the cavities and thickness of the panels in order to maximize the total absorption of MPMPs from 100 Hz to 1 kHz. The impedance translation method and a spectral analysis of the MPMPs' scattering matrix have been implemented. Their effective properties are also examined. The optimization process succeeds in compensating for the absorption losses induced by the volumetric modes of the panels, except for those due to the first mode, which is strongly coupled to the acoustic resonances. An optimal decrease in perforation diameter remains the most effective strategy for merging resonances at low and medium frequencies, while an adequate increase of the holes pitch is more suitable for medium frequencies. These mechanical and geometrical parameters must be taken into account when optimizing MPMPs, depending on the frequency range targeted.

1 Introduction

Noise reduction at low frequencies is a recurrent subject of research for improving passive methods without addition of extra mass or space [1]. Low frequency components are predominant for tire rolling noise of vehicles in urban environments [2], noise generated by the aircraft turbo-engines due to their ultra-high bypass ratio [3] or rotating machines in industry [4] associated to combustion engines, gas turbines or HVAC systems [5].

To avoid the application of classical porous materials, the use of Micro-Perforated Panels (MPPs) has been proposed as a non-fibrous alternative [6,7] that combine characteristics of reactive and dissipative devices. MPP absorbers consist of panels perforated with holes of sub-millimeter diameter, situated in front of a rigid or flexible backing wall. One important property of backed MPPs is the fact that they are tunable control devices. Optimal performance can be achieved by a proper selection of their physical constitutive parameters, such as the panel thickness, the size and shape of the perforations, the perforation ratio and the cavity depth [8].

To make the performance frequency band broader, multiple layers of parallels or series perforated and micro-perforated partitions have been considered. Previous works have focussed on sound transmission blockage by multi-layer perforates under normal or oblique incidence. The study of two perforates separated by a thin air gap, the so-called double fishnet, showed a transmission blockage at the frequency $f_b \approx c_0/(2.45\Lambda)$ for a wide range of panel thicknesses d_p and air gap widths d_g, with c_0 the air sound speed and Λ the holes spacing [9,10]. This blockage is due to coupling between the odd-order modes of the open-ended pipes, constituted by two aligned holes, with the resonant side-branch due to the air gap at the pipe mid-point.

In order to broaden the frequency bandwidth of transmission blockage, a structure composed of multilayer periodically-spaced perforated panels [Figure 1] has been studied [11] and its transmission properties verified experimentally under normal incidence. The parametric studies showed that the broadest stop band occurred for equal panel and gap thicknesses and for panels with a low perforation ratio. Sound transmission stop bands and pass bands were predicted by Bloch-Floquet analysis and observed up to 20 kHz when increasing the number of perforated panels, but at the expense of large reflections.

In order to overcome this limitation, a functionally-graded micro-perforated partition with sole monotonic axial variation of the MPP holes across the partition depth, keeping fixed the MPP and air gap parameters has been studied [12]. As for micro-perforated partitions, the assumption of rigid structures is often limited by the sub-millimetric thickness of the constituting membranes [13] or by the modal behaviour of the individual plates [14]. These structural effects, such as coupling local resonators with an elastic panel, may be beneficial to broaden the efficiency range [15], but they may also be detrimental, especially if the structural and the hole-cavity resonances are strongly coupled with each other [12].

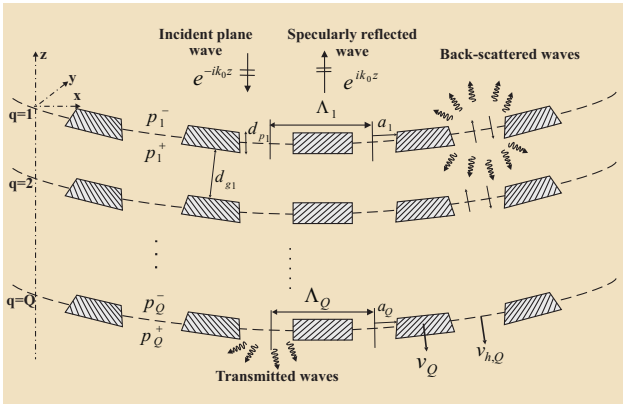

Figure 1 – Cross-view of a multi-layered functionally-graded micro-perforated vibrating partition with physical parameters that vary between layers.

The present work focuses on the idea of optimizing the absorption and transmission properties of a functionally-graded material made up of alternating layers of air and perforated plates whose local filling fraction, $\varphi_f = d_p(1-\sigma)/(d_p + d_g)$ that depends on the perforation ratio σ, can be varied along the propagation direction. The acoustical properties are analyzed under normal incidence and the vibrational effects are included considering two approximations: the elastic membrane and the modal formulation, presented in Section 2. These approaches are compared in Section 3 for the optimal selection of the rigid or vibrating physical parameters constituting the multi-layer absorbers. A critical coupling analysis of the scattering matrix that relates the outgoing and ingoing amplitudes of the two-port partitions is also presented to obtain further insights on the damping mechanism and the improvement of the dissipation plateau. A summary of the main conclusions and some ideas for future work are outlined in the last section.

2 Impedance translation approach

An analytic formulation to account for elasticity and modal response of MPPs using an impedance translation approach is presented in this section. We consider a series of Q rigid or elastic MPPs as sketched in Figure 1. They are characterized by their thickness $d_{p,q}$, their holes diameter $d_{h,q} = 2a_q$ with a_q the holes radius, and their perforation ratio $\sigma_q = \pi d_{h,q}^2/(4\Lambda_q^2)$ with Λ_q the holes pitch. The MPPs are separated by $(Q-1)$ air layers of constant depth $d_{g,q} = D$ for this study. In case of an acoustic fishnet, the holes diameter stays constant across the partition such that $d_{h,q} = d$. As for functionally-graded (FG) micro-perforated partitions, it monotonically decreases from the front to the back panel, such that $d_{h,q+1} = d_{h,q} - c_q\Lambda_q/2$, $q = 1,\ldots,Q$, with c_q the rate of decay for the holes diameter. The front panel is insonified by a normal incident plane wave and the back panel radiates a plane wave in free-field.

The impedance translation approach (ITA) provides a recursive relationship for the effective input impedance of each panel-cavity layer, $Z_{\text{input},q}$ ($q = 1,\ldots,Q-1$),

$$Z_{\text{input},q} = Z_{\text{MPP},q} + Z_0\frac{Z_{\text{input},q+1}\cos(k_0 d_{g,q}) + \mathrm{j}Z_0\sin(k_0 d_{g,q})}{Z_0\cos(k_0 d_{g,q}) + \mathrm{j}Z_{\text{input},q+1}\sin(k_0 d_{g,q})}, \quad (1)$$

obtained from particle velocity and acoustic pressure continuity over the MPP-air layer interfaces, with $k_0 = \omega/c_0$ the acoustic wavenumber, ω the angular frequency, $Z_0 = \rho_0 c_0$ the air characteristic impedance, ρ_0 the air density and $Z_{\text{input},Q} = Z_{\text{MPP},Q} + Z_0$ the input impedance of the transmitting back panel. The normal incidence reflection coefficient is obtained as $r = \left|(Z_{\text{input},1} - Z_0)/(Z_{\text{input},1} + Z_0)\right|^2$. The transmitted power τ reads $\left|2Z_{Q/1}/(Z_{\text{input},1} + Z_0)\right|^2$ with $Z_{Q/1}$ the transfer impedance across the whole partition,

$$Z_{Q/1} = Z_0\prod_{q=1}^{Q-1}\frac{Z_0}{Z_0\cos(k_0 d_{g,q}) + \mathrm{j}Z_{\text{input},q+1}\sin(k_0 d_{g,q})}. \quad (2)$$

The dissipation coefficient is given by $1 - r - \tau$ and the Transmission Loss (TL) is defined as $-20\log_{10}(\tau)$.

For a rigid MPPs with zero air particle axial velocity at the holes walls, the effective transfer impedance of the q^{th} MPP, $Z_{\text{MPP},q} = (p_q^- - p_q^+)/\sigma_q v_{h,q}$, can be written as the sum of an inner term,

$$Z_{\text{in},q} = -\mathrm{j}\omega\rho_0 d_{p,q}\left[\sigma_q\left(1 - G(\mathrm{Sh}_{h,q}\sqrt{\mathrm{j}})\right)\right]^{-1}, \quad (3)$$

and an outer term,

$$Z_{\text{ext},q} = \sigma_q^{-1}\left[\sqrt{2}\eta\,\mathrm{Sh}_{h,q}/d_{h,q} - \mathrm{j}\omega\rho_0 8d_{h,q}/(3\pi)\right], \quad (4)$$

so that $Z_{\text{MPP},q} = Z_{\text{in},q} + Z_{\text{ext},q}$ with the holes Shear number $\mathrm{Sh}_{h,q} = d_{h,q}\sqrt{\omega\rho_0/(4\eta)}$, the air dynamic viscosity η and $G(u) = 2J_1(u)/[uJ_0(u)]$ with J_1 and J_0 Bessel functions of orders 0 and 1. Eqs. (3) and (4) describe the frictional and reactive mass effects taking place respectively within and at the inlet/outlet of the MPP holes [6].

2.1 Limp elastic partitions

One considers limp elastic micro-perforated partitions (EMP) of infinite lateral extent. If one applies continuity at the apertures boundary between the in-hole air-particle velocity and the wall normal velocity, one obtains the following expression for the overall transfer impedance of EMPs, $Z_{\text{EMP},q} = (p_q^- - p_q^+)/[\sigma_q v_{h,q} + (1-\sigma_q)v_q]$, under normal incidence [13]

$$Z_{\text{EMP},q} = Z_{\text{ext},q} + \left\{\frac{1}{Z_{\text{in},q}} + \mathrm{j}\frac{G(\mathrm{Sh}_{h,q}\sqrt{\mathrm{j}})}{\omega\rho_{\mathrm{P}} d_{p,q}}\right\}^{-1}, \quad (5)$$

with ρ_{P} the material density.

2.2 Modal partition analysis

One now assumes that the partition is made up of simply-supported finite-sized MPPs of length a and width b. Under normal incidence, only the resonant volumetric modes of odd orders contribute to the panels structural admittance $Y_{\mathrm{P},q}$, thus yielding

$$Y_{\mathrm{P},q} = \frac{-\mathrm{j}\omega}{\rho_{\mathrm{P}} d_{p,q}} \sum_{\substack{m'n' \\ \text{odd}}} \frac{16}{m'^2 n'^2 \pi^4} \frac{1}{\omega_{m'n'}^2 - \omega^2 - 2\mathrm{j}\xi_{m'n'}\omega_{m'n'}\omega}, \quad (6)$$

with $\omega_{m'n'} = 2\pi f_{m'n'} \sqrt{(1-\sigma_q)/[1+(2-3\upsilon_{\mathrm{P}})\sigma_q]}$ the angular resonance frequency related to the panel mode of order $m'n'$, the resonance frequency of the unperforated panel $f_{m'n'} = (\pi/2)\sqrt{D_{\mathrm{P}}/(\rho_{\mathrm{P}} d_{p,q})}\left[(m'/a)^2 + (n'/b)^2\right]$ and $\xi_{m'n'}$ the corresponding modal damping factor. D_{P} is the panel flexural rigidity. The effect of the MPPs volumetric mode is taken into account through an extended transfer impedance, $\tilde{Z}_{\mathrm{MPP},q} = Z_{\mathrm{EMP},q}\left(Z_{\mathrm{EMP},q} Y_{\mathrm{P},q} + 1\right)^{-1}$, with $Z_{\mathrm{EMP},q}$ and $Y_{\mathrm{P},q}$ given respectively by Eqs. (5) and (6).

3 Acoustic optimisation results

Simulations have been carried out to assess the effects of MPPs first volumetric modes and elasticity on the acoustic performance of optimized MPMPs undergoing a normal incidence excitation. The dissipation, reflection and transmission loss have been calculated from the impedance translation approach (Sec. 2) for functionally-graded MPMPs whose axial rate of decay of the porosity and filling fraction has been optimised to achieve maximal total dissipation frequency-averaged between 100 Hz and 1 kHz. The MPMPs are made up of Q = 20 MPPs of thickness $d_{p,q}$ = 0.5 mm, separated by air gaps of depth $d_{g,q} = D$ = 15.3 mm, so that the overall length is L= 300.7 mm. The decrease of perforation ratio σ_q across the partition is achieved either by optimal decrease of the holes diameter $d_{h,q}$ and constant holes pitch $\Lambda_q = \Lambda$ = 10 mm, or by optimal increase of the holes pitch Λ_q and constant holes diameter set to $d_{h,q} = d$ = 0.45 mm, from the front side to the back side of the MPMP.

Another strategy has been assessed optimizing the increase of the axial filling fraction across the partition, $f_q = d_{p,q}/(d_{p,q} + d_{g,q})$, while keeping a constant panel-air gap thickness $d_{p,q} + d_{g,q}$ = 15.8 mm, together with the hole-based negative porosity. A global search method based on simulated annealing optimization algorithm has been used to find the optimum decrease of the perforation ratio σ_q or the optimal increase of axial filling fraction f_q assuming either rigid MPP partitions, or elastic EMPs vibrating on their first structural modes.

3.1 Optimization of rigid MPP partition

Assuming rigid MPPs with transfer impedance $Z_{\mathrm{MPP},q}$, the red curves in Figure 2 show that the optimization successfully provides grouping and merging of a number of Hole-Cavity (HC) resonances up to 1 kHz, in order to achieve broadband dissipation values that stay above 0.9 between 130 Hz and 1326 Hz as well as a low reflection coefficient that does not exceed 0.1 over this bandwidth that covers the low and medium frequency range. The full width at 50% maximum (FW50M) covers 2350 Hz as from 95 Hz. The high dissipation and low reflection coefficients up to 1 kHz are respectively associated to large impedance matching and substantial visco-thermal dissipation of the incident wave as it enters the partition through the MPP holes.

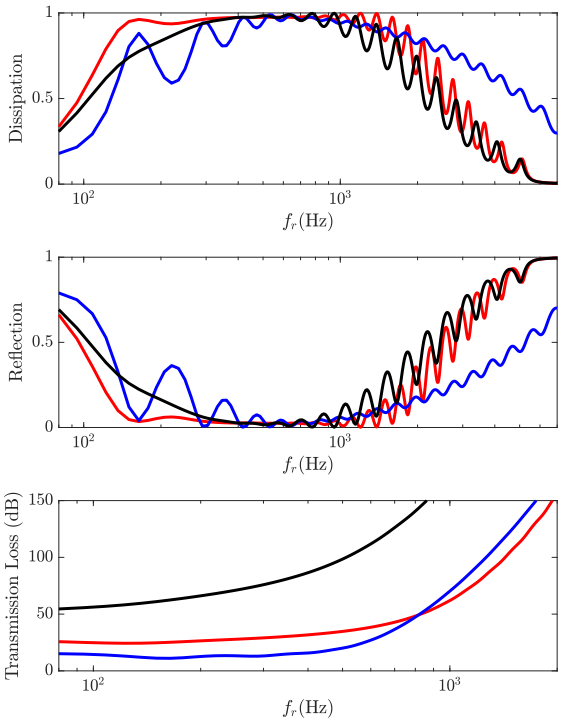

Figure 2 – Dissipation (top), reflection (middle) and transmission loss (bottom) of a rigid MPMP under normal incidence with optimized porosity gradient (holes diameter, red; holes pitch, blue) and axial filling fraction (black) between 100 Hz and 1 kHz.

These performance are associated to an exponential decay of the holes diameters from 4 mm on the front MPP down to 0.12 mm on the transmitting MPP, corresponding to a linear decay of the holes diameter (in logarithmic scale) along the MPPs axial positions. This decay of the holes diameter corresponds to an optimal decrease of the perforation ratio from 50.2% on the front side to 0.05% on the back side of the partition. Hence, due to minute transmission of the incident energy by the back MPP with very low porosity, the TL already achieves 25 dB at 100 Hz and steadily increases above 1 kHz.

This axial drop of the porosity can also be achieved by increasing the holes pitch across the partition from 1.1 mm on the front side to 37.6 mm on the back side, which is easier to achieve in terms of manufacturing process. Note that interaction effects between adjacent holes have been accounted for in $Z_{\mathrm{MPP},q}$ through the Fok's correction factor [16]. This second strategy (blue curves in Figure 2) leads to

high dissipation values that stay above 0.9 from 388 Hz to 1536 Hz, minute reflection over this bandwidth and an almost constant TL of 11dB up to 780 Hz, that rises as frequency increases above 780 Hz. The FW50M covers 4950 Hz as from 130 Hz, which is about twice the FW50M due to decrease of the holes diameter. Exponential increase of the holes pitch thus provides a distinct effect with respect to exponential decrease of the holes diameters, although they both correspond to the same decay of porosity across the partition. The latter strategy favors merging of the HC resonances over a broader frequency range whose central frequency is upshifted by 220 Hz with respect to the former approach.

The third strategy based on optimal increase of the axial filling fraction and decrease of the hole-based porosity across the partition (black curves in Figure 1) produces high dissipation values above 0.9 from 250 Hz to 1 kHz together with small reflection (less than 10%) over this frequency range. The FW50M covers 1890 Hz above 110 Hz. The associated efficiency bandwidth is reduced with respect to that solely due to hole-based negative porosity, especially at low frequencies below 300 Hz. Optimal axial increase of the filling fraction from 3% to 32% across the partition degrades the impedance matching performance below 300 Hz and above 700 Hz, resulting in larger back-reflections over these bandwidths with respect to the hole-based strategy (red curves), as seen in Figure 2. Moreover, the filling fraction approach induces higher dissipation at the HC resonances activated between 300 Hz and 700 Hz whereas larger reflections are observed in-between. Overall, this results in large TL values that exceed those due to hole-based negative porosity by 30 dB at 100 Hz and by 100 dB at 900 Hz. These TL performance however require the delicate manufacturing of thick panels with sub-millimetric holes diameter.

3.2 Optimization of vibrating MPP partition

One considers a MPMP made up of finite-sized simply-supported aluminum MPPs of length 0.3 m, width 0.2 m and with a modal damping factor of 1%. One neglects the added structural damping induced by the micro-perforations [17], but one accounts for the decrease of the panel resonance frequencies due to an increase of the perforation ratio, as modelled in Sec. 2.2. A number of 18 × 18 structural modes have been accounted for so that the front MPP with the largest porosity is structurally resonant up to 7.4 kHz. Due to the normal incidence, only volumetric modes are activated.

Figure 3 shows that, compared to the rigid case, the optimization process is still able to provide high broadband dissipation and minute reflections over similar bandwidths when accounting for the modal response of elastic MPPs. The optimal gradient of porosity and filling fraction is comparable (within less than 1%) to the optimal parameters in the rigid case, showing robustness of the optimized parameters to the effect of the volumetric modes.

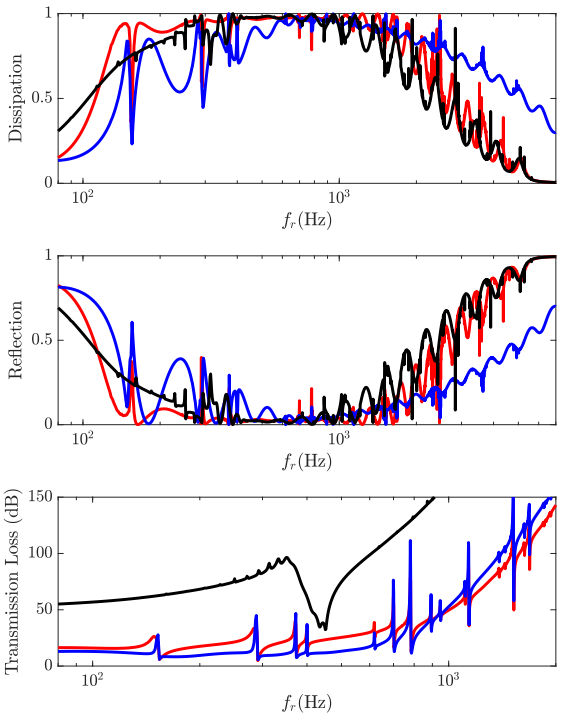

Figure 3 – Dissipation (top), reflection (middle) and transmission loss (bottom) of an elastic MPMP responding under normal incidence on its first 18 × 18 modes with optimized porosity gradient (holes diameter, red; holes pitch, blue) and filling fraction (black) between 100 Hz and 1 kHz.

Figure 3 also shows that the trends observed in Figure 2 on the MPMP acoustical properties are preserved, except locally where coupling between the Panel-Cavity (PC) vibroacoustic modes and HC acoustic modes produces dips and peaks in the dissipation, reflection and TL curves. The volumetric modes induce dissipation dips and reflection peaks typically below 1 kHz whereas the reverse trend is observed above 1 kHz, with dissipation peaks and reflection dips. The situation is different for the TL with local TL peaks, immediately followed by TL dips. They can be seen in Figure 3 (red and blue curves) for the porosity gradient strategy. The black TL curve related to the filling fraction optimisation shows a weak modal behavior, mostly encapsulated in the dissipation and reflection properties. A significant TL drop is observed between 400 Hz and 500 Hz, where the TL is essentially driven by visco-thermal dissipation with stronger merging between the HC resonances with respect to sole optimization of the porosity gradient. Out of this range, reactive effects due to back-reflections are prominent and provide higher TL values.

3.3 Critical coupling analysis

Further insights can be gained on the optimized MPMP performance and the effects of the volumetric MPP modes from critical coupling analysis [18] of the scattering S-matrix that relates the outgoing and ingoing amplitudes of the MPMP two-port partition. Perfect dissipation is achieved if

the two eigenvalues of the S-matrix are zero-valued at the same real frequency. Only the first eigenvalue (in logarithmic scale) has been plotted in Figures 4 to 6 that show a distribution of zero-poles in the complex frequency plane (f_r, f_i). Zeros in the lower- (resp. upper-) half-planes, such that $f_i < 0$ (resp. $f_i > 0$), are related to over- (resp. under-) resistive resonances.

Non-optimized rigid MPMP partitions (not shown) typically exhibit distinct dissipation peaks associated to under-damped HC resonances distributed over the whole spectrum. Figure 4 shows that the optimization process related to negative porosity gradient reallocates the amount of damping (downshift along the f_i - axis) and the spectral distribution (compression towards the low-frequencies along the f_r - axis) of the HC resonances related to zero-pole pairs. These HC resonances belong to three groups. Assuming variations of the holes diameter, one obtains 7 over-damped resonances below 900 Hz, one critically-coupled (CC) resonance at 1 kHz that leads unit dissipation and 11 under-damped resonances above 1 kHz. As for holes pitch variations, one observes 3 over-damped resonances below 450 Hz, one critically-coupled (CC) resonance at 523 Hz and 13 under-damped resonances above 600 Hz.

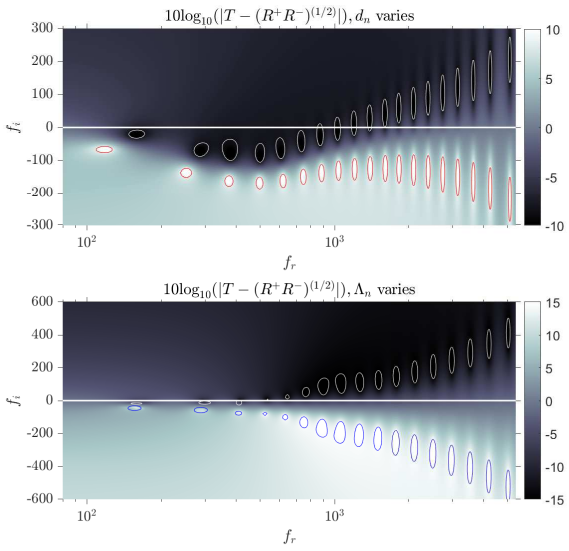

Figure 4 – Effect of optimizing the porosity gradient of a rigid MPMP (holes diameter, top; holes pitch, bottom) on the modulus (log10 values) of the S-matrix first eigenvalue in the complex frequency plane with T, R^- and R^+ the transmission, left and right reflection coefficients; isocontours are also shown around the zeros (- 8 dB, top; - 15 dB, bottom) and the poles (8 dB, top; 15 dB, bottom).

Figures 5 and 6 show that the optimized performance of MPMPs vibrating on their first volumetric modes modifies the distribution of zero-pole pairs in the complex frequency plane.

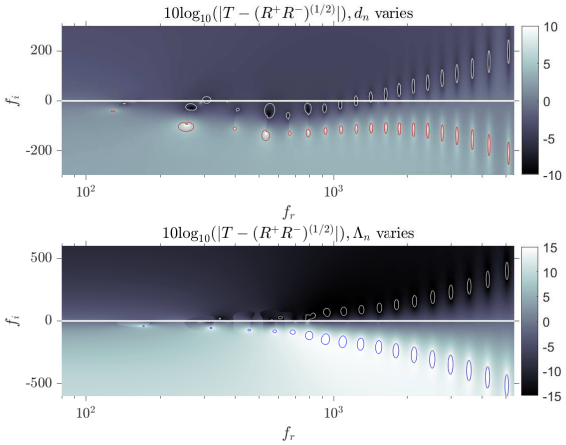

Figure 5 – Effect of optimizing the porosity gradient of a rigid MPMP (holes diameter, top; holes pitch, bottom) on the modulus (log10 values) of the S-matrix first eigenvalue in the complex frequency plane with T, R^- and R^+ the transmission, left and right reflection coefficients; isocontours are also shown around the zeros (- 8 dB, top; - 15 dB, bottom) and the poles (8 dB, top; 15 dB, bottom).

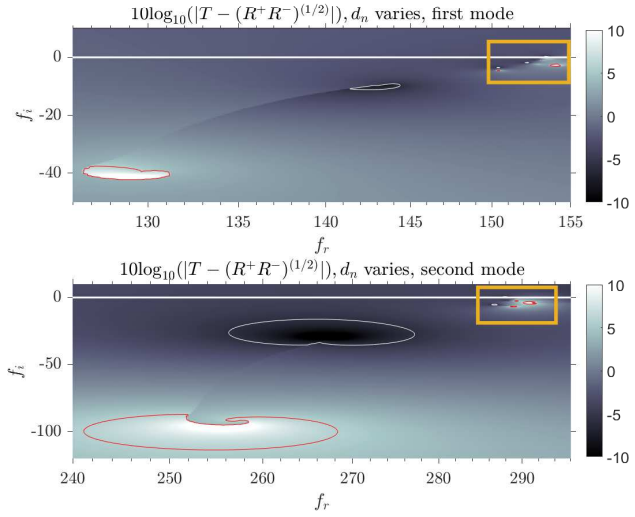

Figure 6 – Effect of the first (top) and second (bottom) panel volumetric modes of the elastic MPMP, whose holes diameter have been optimized, on the modulus (log10 values) of its S-matrix first eigenvalue in the complex frequency plane; panel – hole – cavity coupled resonances are located within the orange rectangles; also shown are isocontours around the zeros (- 5.8 dB, top) and the poles (5.8 dB, bottom).

Strong coupling between the PC volumetric modes and the neighboring HC over-damped resonances leads to resonance splitting and the emergence of Panel-Hole-Cavity (PHC) resonances. They are related to the zero-pole pairs located within the orange rectangles of Figure 6 for the first two HC resonances. Accumulation of the PHC poles close to the real frequency axis at 155 Hz and 290 Hz leads to local drops of dissipation in Figure 3 below 900 Hz, which are not compensated by the optimization process. These drops in

dissipation are accompanied by local peaks in reflection and decrease of the TL. Figure 5 shows that occurrence of the zero-pole pairs near the frequency axis is observed for both holes diameter and holes pitch strategies. Above 1 kHz, the PHC resonances are under-resistive and HC-controlled. Adding losses by considering MPPs made up of visco-elastic materials would *a priori* be beneficial to balance the amount of leakage for these resonances and ensure a higher dissipation performance.

4 Conclusions

This study analyzes how the Hole-Cavity resonances of multilayered MPP partitions are modified by the volumetric elastic panel modes after optimization of the porosity or filling fraction gradients. It is based on the cost-efficient impedance translation approach and on the critical coupling analysis of coupling between the hole-cavity and panel-cavity resonances.

It is found that optimisation of the holes diameter in order to achieve negative porosity gradient provides the best performance results with broadband high dissipation, minute reflections and a TL above 25 dB over the low- and mid-frequency ranges. Holes pitch optimization is more suitable to achieve high performance in the mid-frequency range. Optimizing the filling fraction as well as the holes diameter degrades the low-frequency performance, but significantly enhances the TL.

Accounting for the MPP structural volumetric modes leads to the emergence of panel-hole-cavity resonances with zero-pole pairs close the real axis. Below 1 kHz, they produce adverse effects with local dissipation dips and reflection peaks that the optimization process is not able to compensate. Above 1 kHz, they produce beneficial effects.

Further studies would consider the ability of visco-elastic MPPs with a suitable amount of added damping to compensate for the adverse effects of the non-optimized volumetric modes.

Acknowledgments

This work is part of the project PID2022-139414OB-I00 funded by MCIN/AEI/10.13039/501100011033/ and by "ERDF A way of making Europe". It has also received support from the French government under the France 2030 investment plan, as part of the Initiative d'Excellence d'Aix-Marseille Université - A*MIDEX (AMX-22-RE-AB-157).

References

[1] F.J. Fahy and P. Gardonio, *Sound and Structural Vibration. Radiation, Transmission and Response*, Academic Press, Oxford (2006).

[2] T. Bravo, An analytical study on the amplification of the tyre rolling noise due to the horn effect, *Applied Acoustics* **123**, 85-92 (2017).

[3] D. Giesecke, M. Lehmler, J. Friedrichs, J. Blinstrub, L. Bertsch and W. Heinze, Evaluation of ultra-high bypass ratio engines for an over-wing aircraft configuration, *Journal of the Global Power and Propulsion Society* **2**, 493-515 (2018).

[4] B. Berglund, P. Hassmén and R.F. Job, Sources and effects of low-frequency noise, *Journal of the Acoustical Society of America* **99**, 2985-3002 (1996).

[5] F. Czwielong, S. Floss, M. Kaltenbacher and S. Becker, Influence of a micro-perforated duct absorber on sound emission and performance of axial fans, *Applied Acoustics* **174**, 107746 (2021).

[6] D.Y. Maa. Potential of microperforated panel absorber, *Journal of the Acoustical Society of America*, **104**, 2861-2866 (1998).

[7] D.Y. Maa, Theory and design of microperforated panel sound-absorbing constructions, *Scientia Sinica* (English edition) **18**, 55-71 (1975).

[8] T. Bravo and C. Maury, Causally-guided acoustic optimization of rigidly-backed micro-perforated partitions: Case studies and experiments, *Journal of Sound and Vibration* **523**, 116735 (2022).

[9] J. Christensen, L. Martinez-Moreno and F.J. Garcia-Vidal, All-angle blockage of sound by an acoustic double-fishnet metamaterial, *Applied Physics Letters* **97**, 134106 (2010).

[10] J. S. Bell, I. R. Summers, A. R. J. Murray, E. Hendry, J. R. Sambles, and A. P. Hibbins, Low acoustic transmittance through a holey structure, *Physical Review B* **85**, 214305 (2012).

[11] N. Aközbek, N. Mattiucci, M. J. Bloemer M. Sanghadasa and G. D'Aguanno, Manipulating the extraordinary acoustic transmission through metamaterial-based acoustic band gap structures, *Applied Physics Letters* **104**, 161906 (2014).

[12] T. Bravo, C. Maury and C. Pinhede, Enhancing sound absorption and transmission through flexible multi-layer micro-perforated structures, *Journal of the Acoustical Society of America* **134**, 3363-3373 (2013).

[13] C. Li, B. Cazzolato and A. Zander, Acoustic impedance of micro perforated membranes: Velocity continuity condition at the perforation boundary, *Journal of the Acoustical Society of America **139**,* 93-103 (2016).

[14] S.W. Ren, L. Van Belle, C. Claeys, F.X. Xin, T.J. Lu, E. Deckers and W. Desmet, Improvement of the sound absorption of flexible micro-perforated panels by local resonances, *Mechanical Systems and Signal Processing* **117**, 138-156 (2019).

[15] Y. Zhang, G. Wang, Z. Zhu, and Q. Liu, Vibro-acoustic coupling characteristics of the microperforated panel with local resonators, *International Journal of Mechanical Sciences* **245**, 128125 (2023).

[16] T.H. Melling, The acoustic impedance of perforates at medium and high sound pressure levels, *Journal of Sound and Vibration* **29**, 1-65 (1973).

[17] L. Gallerand, M. Legrand, T. Dupont and P. Leclaire, Vibration and damping analysis of a thin finite-size microperforated plate, *Journal of Sound and Vibration*, **541**, 117295 (2022).

[18] V. Romero-García, G. Theocharis, O. Richoux, A. Merkel, V. Tournat and V. Pagneux, Perfect and broadband acoustic absorption by critically coupled sub-wavelength resonators, *Scientific Reports* **6**, 19519 (2016).